

Supporting Information

Manipulating the dimensional assembly pattern and crystalline structure of iron oxide nanostructures with a functional polyolefin

Qingliang He,^a Tingting Yuan,^a Yiran Wang,^a Abhishant Guleria,^b Suying Wei,^{*b} Guoqi Zhang,^{*c} Luyi Sun,^d Jingjing Liu,^d Jingfang Yu,^d David P. Young,^e Hongfei Lin,^f Airat Khasanov^g and Zhanhu Guo^{*a}

Contents

S1. Experimental

S1.1. Materials

S1.2. Synthesis of Fe₂O₃ NPs with different sizes and assembly patterns

S2.Characterization

Transmission Electron Microscopy (TEM)

Scanning Electron Microscopy (SEM)

X-ray Diffraction (XRD)

X-ray Photoelectron Spectroscopy (XPS)

Fourier Transform Infrared Spectroscopy (FT-IR)

Room Temperature Mössbauer Spectra (MS)

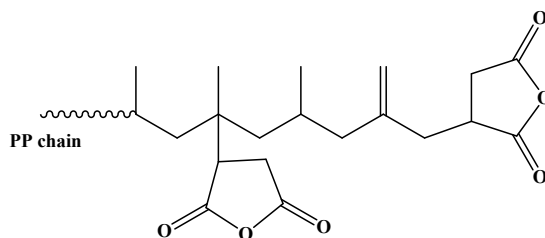
Magnetization Test

Thermo-gravimetric Analysis (TGA)

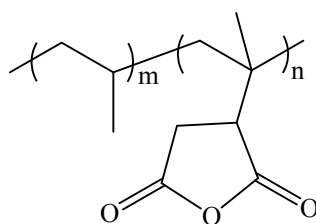
S1. Experimental

S1.1. Materials

The regular PP used here was an isotactic polypropylene ($M_n \approx 40500$), supplied by Total Petrochemicals USA, Inc. PP-g-MA (CAS# 25722-45-6 with $M_n \approx 3900$ and MA: 8-10 wt. %) was purchased from Sigma Aldrich. PP-g-MA was a propylene homopolymer with a maleic anhydride group grafting on its main chain (shown in scheme S2). Iron(0) pentacarbonyl ($\text{Fe}(\text{CO})_5$, 99%) was purchased from Sigma Aldrich. Solvent xylene (laboratory grade, $\rho = 0.87 \text{ g/cm}^3$) was obtained from Fisher Scientific. All the chemicals were used as-received without any further treatment.



Scheme S1. Chemical structure of the specially made PP-g-MA ($M_n \approx 8000$).



Scheme S2. Chemical structure of the commercial PP-g-MA ($M_n \approx 3900$).

S1.2. Synthesis of Fe_2O_3 nanoparticles (NPs) with different sizes and assembly patterns

The detailed synthesis procedures were as follows. The synthesis of quasi-monodispersed Fe_2O_3 NPs (in 2-D assembly pattern): PP-g-MA (1.0 g) and 100 mL xylene were loaded into a 250 mL three-neck flask and heated to reflux while maintained refluxing for 30 min to completely dissolve PP-g-MA. $\text{Fe}(\text{CO})_5$ (3.5 g) was then injected into the hot solution, and the

solution immediately became yellow. The mixture solution formed a black colloidal solution upon refluxing for 3 hours. After cooling down to room temperature in the flask, the black colloidal solution was poured onto a large glass container to evaporate xylene in a fume hood. The evaporation of solvent refers to the slow removal of solvent after the reaction to receive the surfactant coated nanoparticles in solid form for characterization. We performed the solvent evaporation in a fume hood instead of using a rotary evaporator, which contributed to the control of surface tension due to the slow process. This slow process was crucial to the 2-D and 3-D assembly pattern; while 1-D nanochain assembly was mainly controlled by the strong magnetic attraction forces. Then the received black solids were further dried in a vacuum oven for 24 hours to form the final composites before testing. For the synthesis of intermediate Fe₂O₃ NPs (in 3-D porous micro-spheres assembly pattern) and the Fe₂O₃ chain-like structures (in 3-D compressed porous micro-spheres assembly pattern), the same procedures were used as above except different amount of PP-g-MA (0.5 or 0.25 g) was used.

For the synthesis of self-assembled 1-D Fe₂O₃ nanochains, the same procedures were used as above except different amount of PP-g-MA (0.125 g) was used. For the Fe₂O₃ NPs synthesized in regular PP matrix, the same procedures as above were employed, while 1.0 g regular PP was used instead of 1.0 g PP-g-MA in 100 mL xylene. Theoretically, 3.5 g Fe(CO)₅ can be thermally decomposed into 1.0 g Fe. Here, with the fixed 3.5 g Fe(CO)₅ amount and different PP-g-MA concentrations, ~ 1.42 g Fe₂O₃ NPs can be produced each batch.

S2.Characterization

For transmission electron microscope (TEM) characterization, one droplet of the diluted colloid solution was dropped onto carbon-film coated copper grids. The samples were observed in a FEI TECNAI G2 F20 microscope at a working voltage of 200 kV. The selected area electron

diffraction (SAED) pattern was recorded a Gatan SC1000 ORIUS CCD camera. In order to deal with the strong center beam, a needle was placed in the center to block the beam for half of the exposure time (2 seconds) and then the needle was immediately removed away from the view area, so that the needle appeared in the pattern, which blocked the center strong beam for half of the total exposure time.

The micro-structures of these as-obtained NPs were evaluated by scanning electron microscope (SEM, JEOL JSM 6700R) in high vacuum mode. The samples were mounted on an aluminum stub by using carbon tape, and then sputtered in a Hummer 6.2 system (15 mA AC for 30 sec) to create ~ 1 nm thick film of Au before imaging.

X-ray diffraction (XRD) analysis was carried out with a Bruker AXS D8 Discover diffractometer operating with a Cu $K\alpha$ radiation source. The XRD results were recorded at 2θ from 5 to 80°.

The compositions of all the samples were analyzed by X-ray Photoelectron Spectroscopy (XPS). XPS measurements were conducted on a Kratos AXIS 165 system. Analysis of each sample started with a quick survey scan in the binding energy range from 1200 to 0 eV at the pass energy level of 40 eV to check all the possible elements existing in the sample, followed by the high-resolution scan of each element at the pass energy level of 160 eV to obtain the compositional results. Both survey scan and high-resolution scans were carried out with a Mono Al X-ray source at the anode of 10 kV and a beam current of 15 mA.

Fourier transform infrared spectroscopy (FT-IR, Tensor 27, Bruker Inc.) with Hyperion 1000 Attenuated total reflection (ATR) microscopy accessory was utilized to characterize the functional groups of PP-g-MA, and the Fe₂O₃ NPs synthesized and stabilized by PP-g-MA over 4000 to 500 cm⁻¹.

The Mössbauer spectrometer was set to produce a high precision Doppler velocity modulation of the source γ radiation. The effects of the Doppler velocity modulation on the absorption of γ radiation were recorded synchronously in the 1024 channels of the multichannel analyzer. The result was 1024 numbers representing the registered gamma quanta (representing a singular quantum) passing through the absorber under the condition of different Doppler velocity. A separate calibration procedure was used to establish the exact correspondence channel-velocity (Spectrometer calibration was performed by measuring a standard α -Fe absorber, which produced a well-known six line spectrum.) The whole velocity range was calibrated using these six velocity points. The shape of the absorption spectrum was fitted to a theoretical model line shape, which was a superposition of singlets, doublets and sextets (^{57}Fe case) of a Lorentzian form. The result was investigated by chi 2 criterion and the theoretical line shape was tailored to fit experimental spectrum by the adjustment of spectral parameters like isomer shift, quadrupole splitting, hyperfine magnetic field and etc.

The magnetic property measurements were carried out in a 9 T physical properties measurement system (PPMS) by Quantum Design at room temperature.

The residue amounts of these magnetic Fe_2O_3 nanostructures were investigated using thermogravimetric analysis (TGA, TA Instruments Q-500). The samples were heated from room temperature to 600 °C at a constant heating rate of 20 °C/min under N_2 gas atmosphere. The flow rate was 60 mL/min.

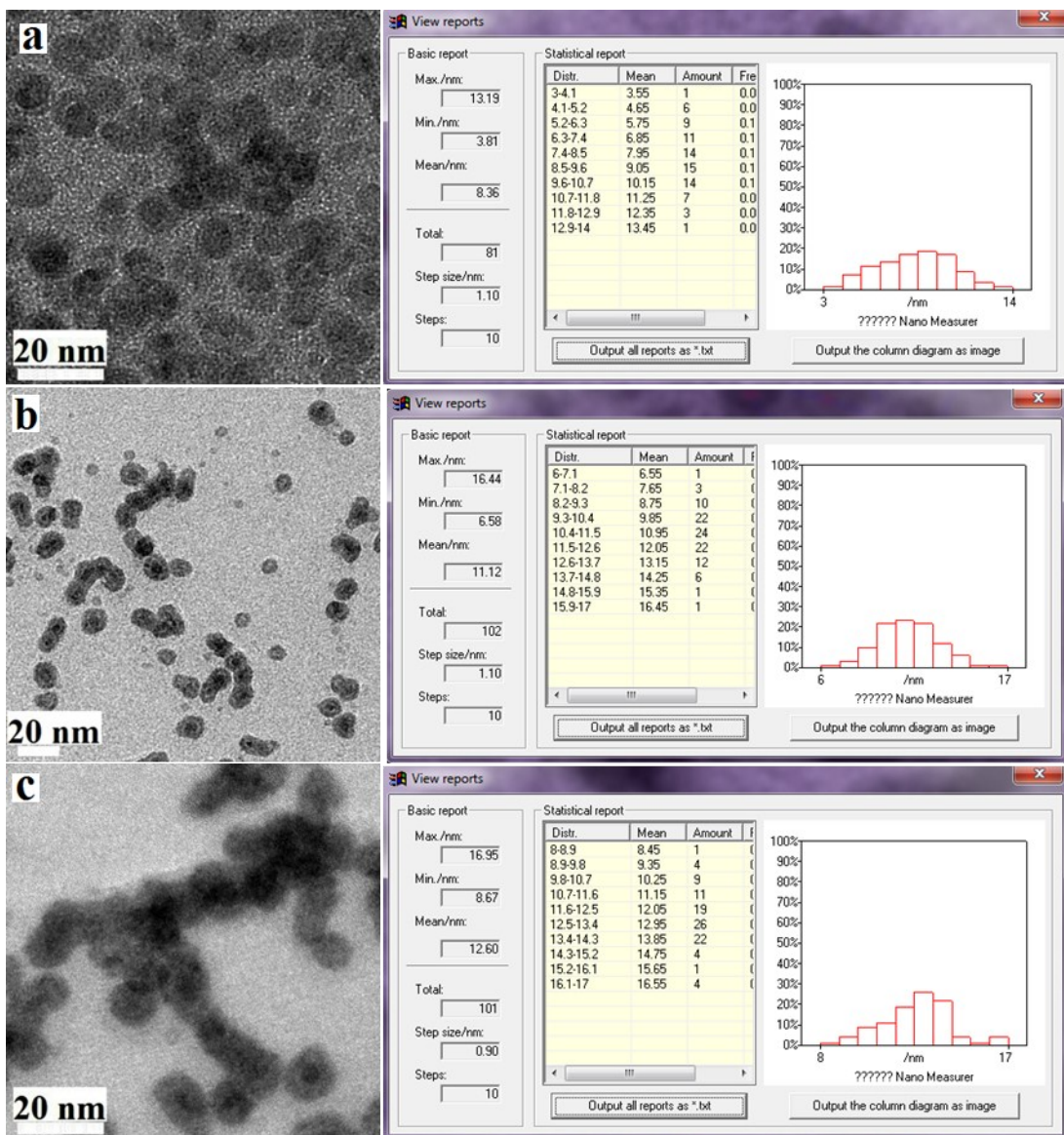


Fig. S1. Particle sizes measured from TEM images using software “Nanomeasurer”: Fe₂O₃ NPs synthesized via thermo-decomposing 3.5 g Fe(CO)₅ in (a). 1.0; (b) 0.5; and (c). 0.25 g PP-g-MA in 100 mL xylene.

For (a): average diameter of 8.4 nm with a total measuring number of 81 particles; (c) average diameter of 11.1 nm with a total measuring number of 102 particles; and (e) average diameter of 12.6 nm with a total measuring number of 101 particles;

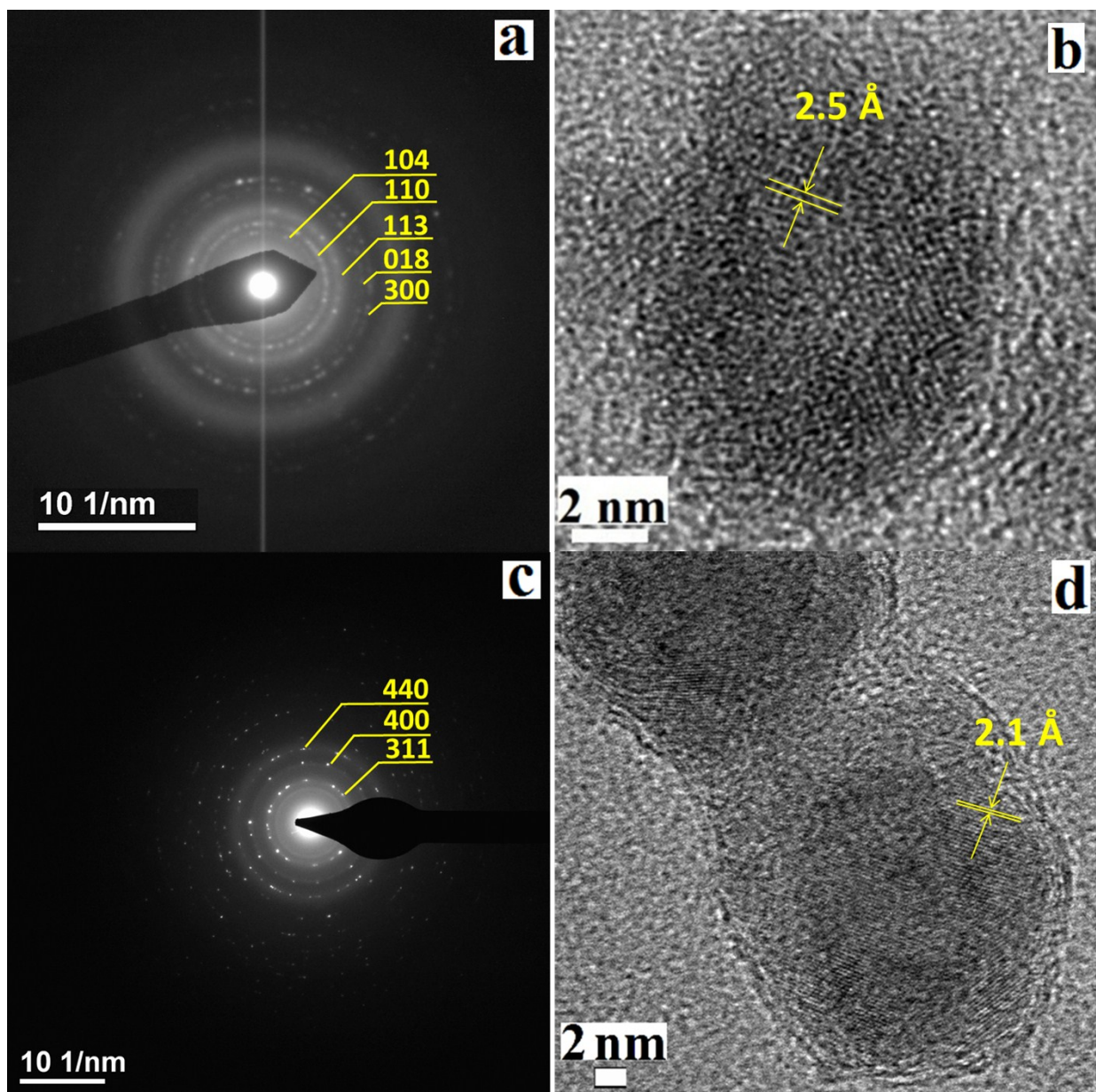


Fig. S2. HR-TEM image and SAED pattern of the Fe_2O_3 NPs synthesized via thermo-decomposing 3.5 g $\text{Fe}(\text{CO})_5$ in 1.0 g (a, b), and 0.125 g (c, d) PP-g-MA in 100 mL xylene.

For the monodispersed NPs, strong ring patterns in Fig. S2a were indexed to (104), (110), (113), (018) and (300) planes of α - Fe_2O_3 (PDF#33-0664); meanwhile, a lattice spacing of 2.5 Å (HR-TEM images shown in Fig. S2b) was measured by software “Nano-measurer”, which can be indexed to the (110) plane of α - Fe_2O_3 (PDF#33-0664).

For the 1-D nanochain, strong ring patterns in Fig. S2c were indexed to (311), (400) and (440) planes of γ - Fe_2O_3 (PDF#39-1346). Additionally, a lattice spacing of 2.1 Å (HR-TEM images shown in Fig. S2d) was measured by software “Nano-measurer”, which can be indexed to the (400) plane of γ - Fe_2O_3 (PDF#39-1346).

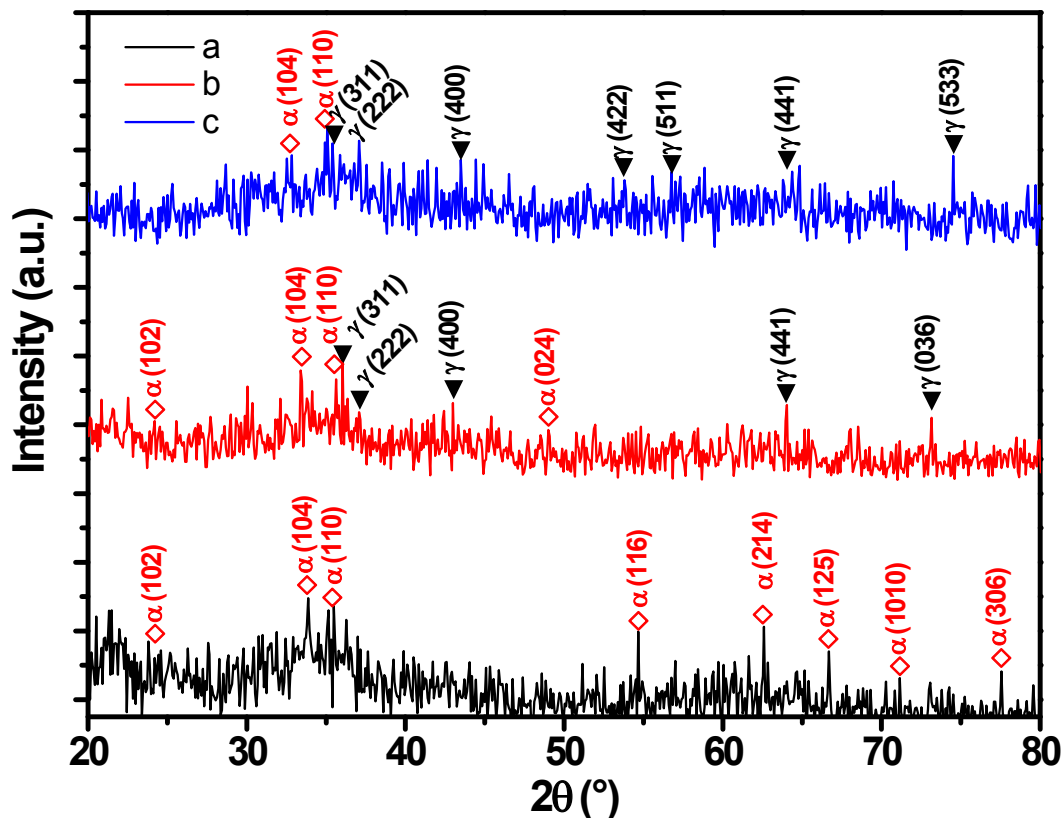


Fig. S3. XRD patterns of the Fe_2O_3 NPs synthesized via thermo-decomposing 3.5 g $\text{Fe}(\text{CO})_5$ in (a). 1.0; (b). 0.5; and (c). 0.25 g PP-g-MA in 100 mL xylene.

The weak and noisy peaks in the XRD data is primarily attributed to the polymorphous and low crystalline NPs synthesized in the in such a mild condition; which can also be confirmed by high resolution transmission electron microscopy (HRTEM) images and the selected area electron diffraction (SAED) patterns.

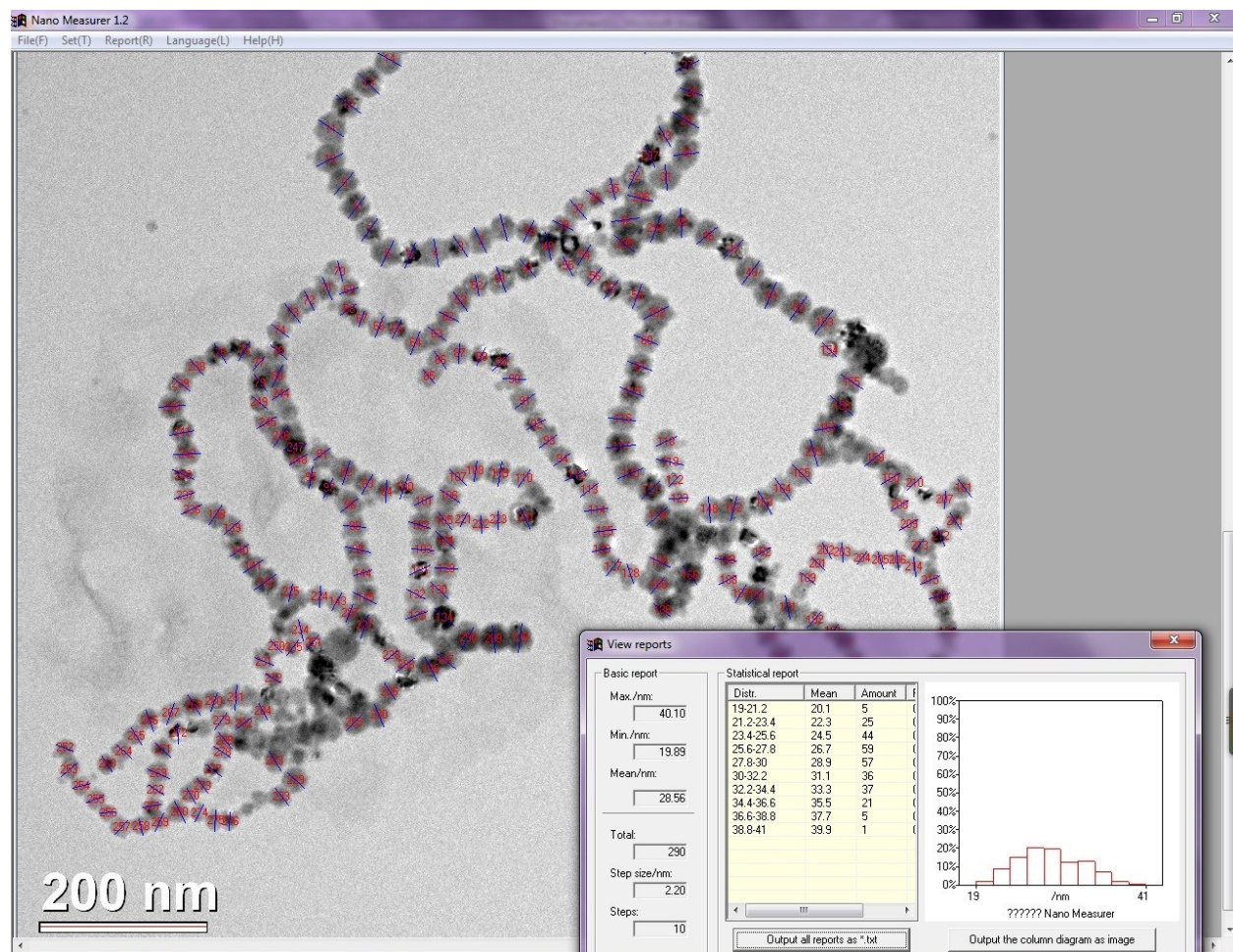


Fig. S4. Particle size of Fe₂O₃ nanochains were measured by software “Nanomeasurer” (NPs synthesized via thermo-decomposing 3.5 g Fe(CO)₅ in 0.125 g PP-g-MA in 100 mL xylene): average diameter of 28.6 nm with a total measuring number of 290 particles.

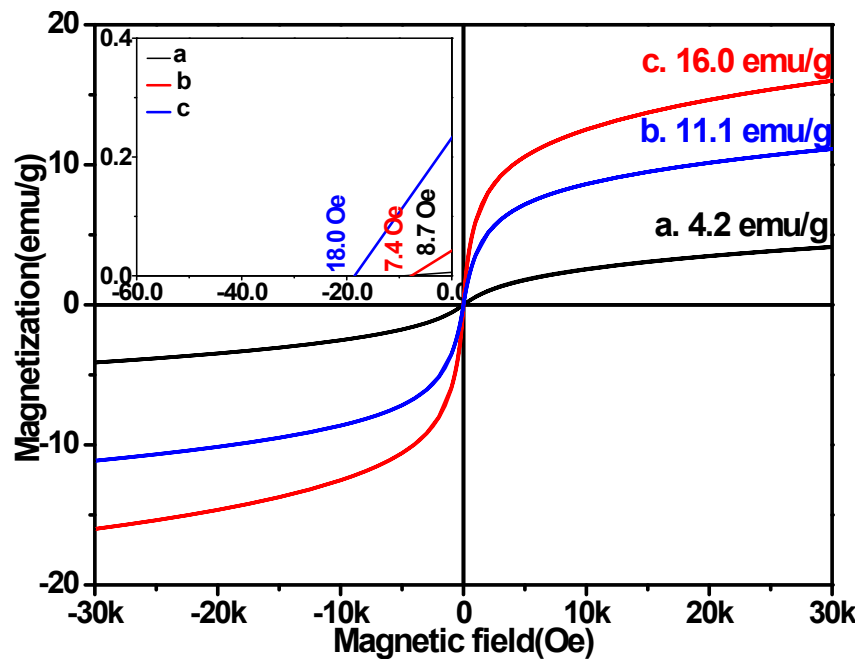


Fig. S5. Room temperature hysteresis loops of the Fe₂O₃ NPs synthesized via thermodecomposing 3.5 g Fe(CO)₅ in (a). 1.0, (b). 0.5, and (c). 0.25 g PP-g-MA in 100 mL xylene.

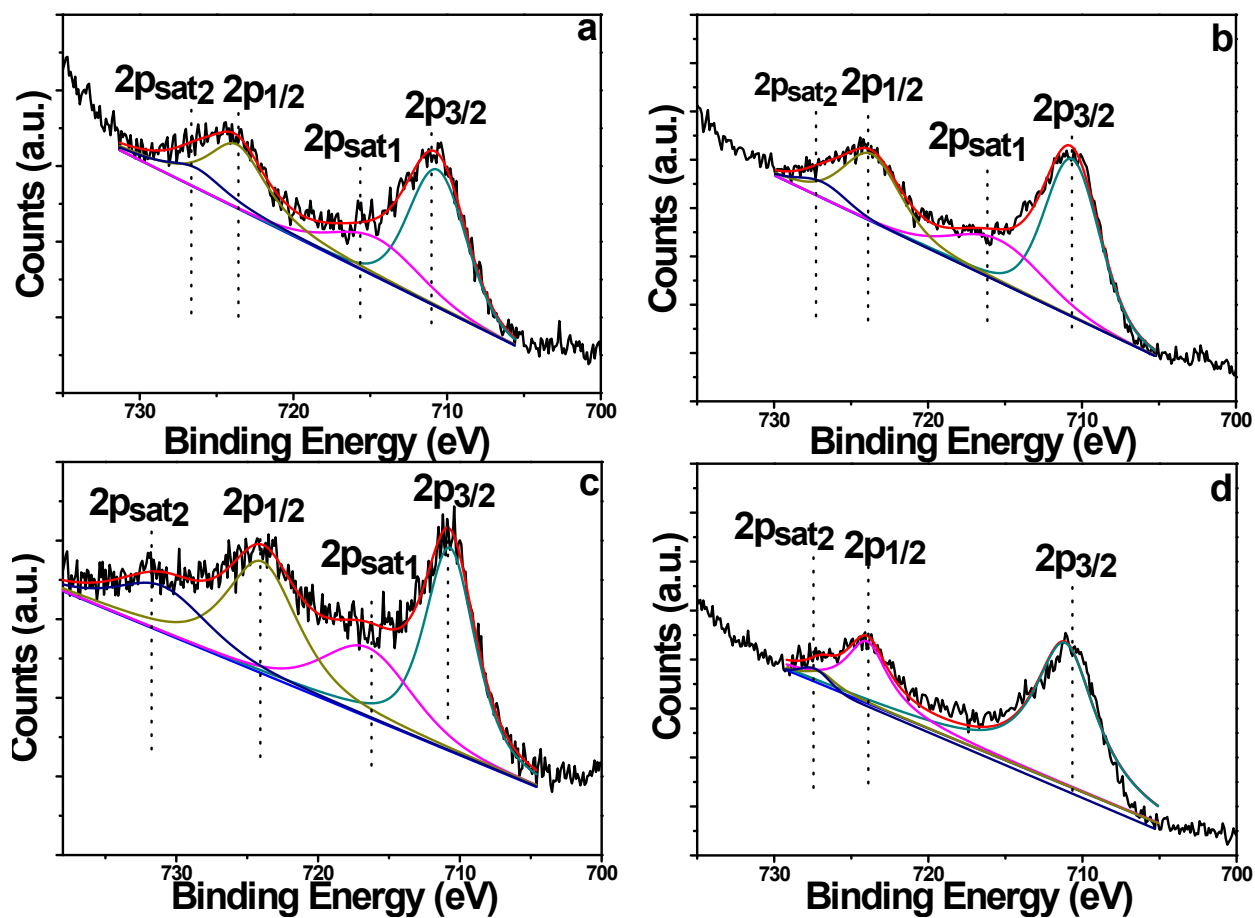


Fig. S6. XPS Fe2p spectra of Fe₂O₃ NPs synthesized via thermo-decomposing 3.5 g Fe(CO)₅ in (a). 1.0; (b). 0.5; (c). 0.25; and (d). 0.125 g PP-g-MA in 100 mL xylene.

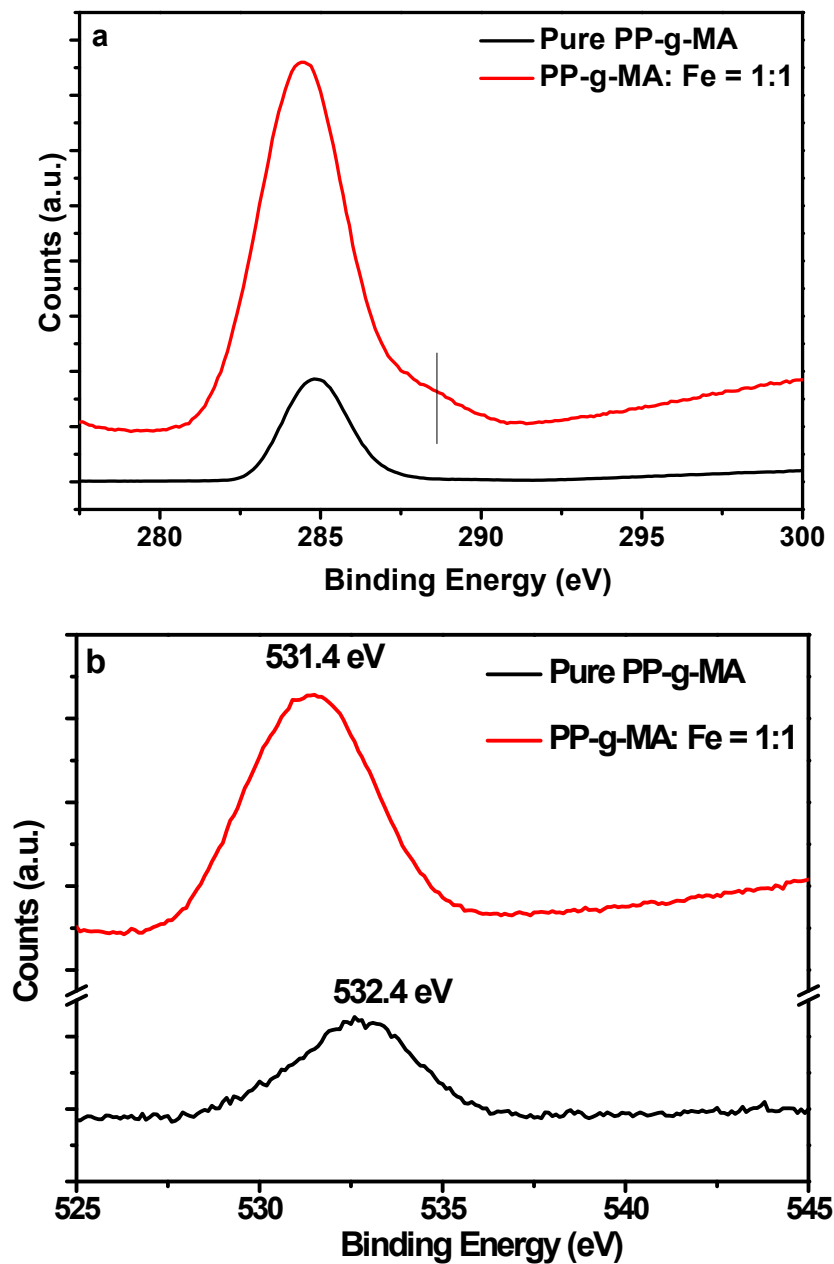


Fig. S7. XPS a) C1s and b) O1s spectra of pure PP-g-MA and Fe₂O₃ NPs synthesized via thermo-decomposing 3.5 g Fe(CO)₅ in 1.0 g PP-g-MA in 100 mL xylene.

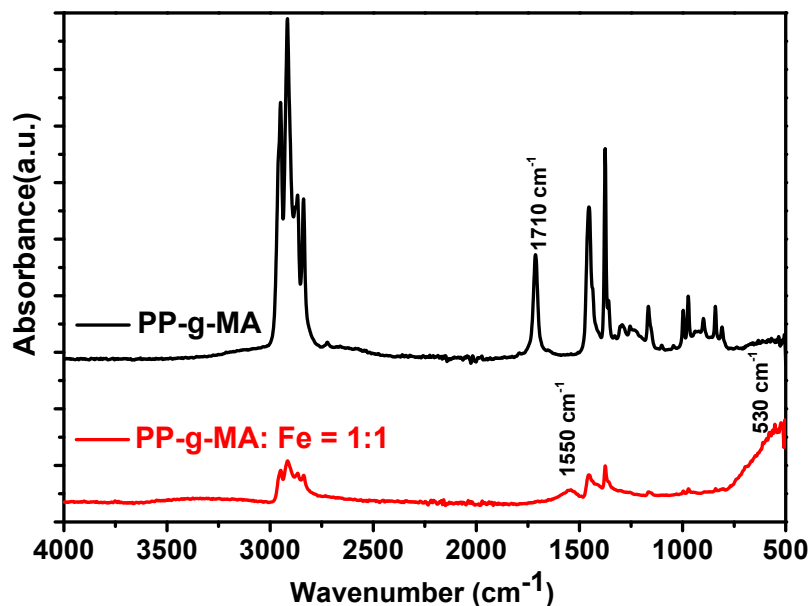
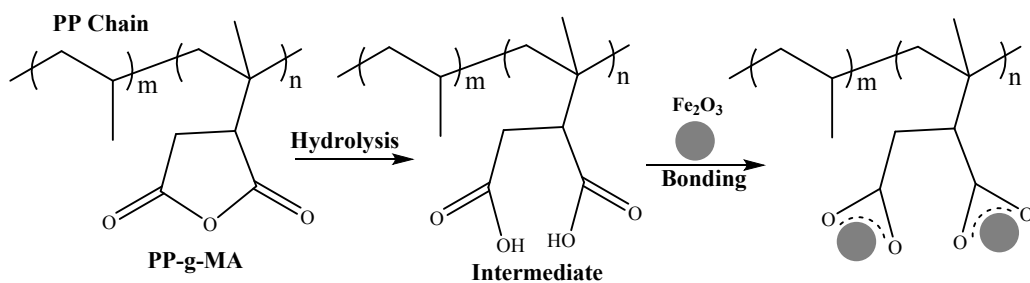


Fig. S8. FT-IR spectra of pure PP-g-MA and monodispersed Fe₂O₃ NPs (NPs synthesized via thermo-decomposing 3.5 g Fe(CO)₅ in 1.0g PP-g-MA in 100 mL xylene).

Only one peak with binding energy at round 284.8 eV was observed for the pure PP-g-MA (Fig. S7a), while two peaks at around 284.0 and 288.0 eV were found for the Fe₂O₃ NPs synthesized with 1.0 g PP-g-MA per 100 mL xylene (XPS C1s spectra, Fig. S7a). The peak around 284.8 eV corresponds to the carbons in the aliphatic chain (here, it corresponds to PP tail in PP-g-MA). The shoulder peak at 288.0 eV is associated to the carboxylate carbon,^{1, 2} confirming that the anhydride has been converted to carboxylate during the synthesis. More importantly, neither of these two peaks can be assigned to a carboxylic carbon, indicating no free carboxylic acid existed on the Fe₂O₃ surface.³ Compared with pure PP-g-MA, the O1s spectrum of the Fe₂O₃ NPs (synthesized with 1.0 g PP-g-MA per 100 mL xylene) depicts a peak shift from 532.4 to 531.4 eV (Fig. S7b). This shift is an direct evidence for the formation of chemical bonds between the Fe₂O₃ and the PP-g-MA via carboxylate bonding.⁴ From FT-IR spectra (Fig. S8), the intensive characteristic C=O absorption peak at 1710 cm⁻¹ was observed for pure PP-g-MA.

For the Fe₂O₃ NPs synthesized with 1.0 g PP-g-MA per 100 mL xylene, it can be observed that the strong C=O absorption peak at 1710 cm⁻¹ disappear totally and a new absorption peak at around 1550 cm⁻¹ is observed. The new peak at 1550 cm⁻¹ is in agreement with the asymmetric and symmetric stretching vibration (CO₂⁻) of carboxylate reported before due to the bonding between carboxyl group and the Fe₂O₃ NPs.⁵⁻⁷ In addition, a new broad absorption peak at around 530 cm⁻¹ is observed, corresponding to the vibration of Fe-O bond in Fe₂O₃.^{8, 9} It is thus clear that carboxylic groups hydrolyzed from maleic anhydride were chemisorbed onto the metal oxide surface. During its dissolution in xylene, PP-g-MA can react with trace amount of moisture in solvent to form carboxylic intermediates, which chemisorbed onto the Fe₂O₃ NPs during thermal decomposition of organometallic precursor in PP-g-MA/xylene solution.¹⁰ Scheme S3 depicts the reaction route. Attributed to the formation of strong bonding between the as synthesized Fe₂O₃ NPs and surfactant PP-g-MA, the large steric hindrance of PP-g-MA long tails provided powerful coordination strength in guiding the crystalline growth of these Fe₂O₃ nanostructures.



Scheme S3. Chemical reaction scheme of bonding Fe₂O₃ NPs by the PP-g-MA.

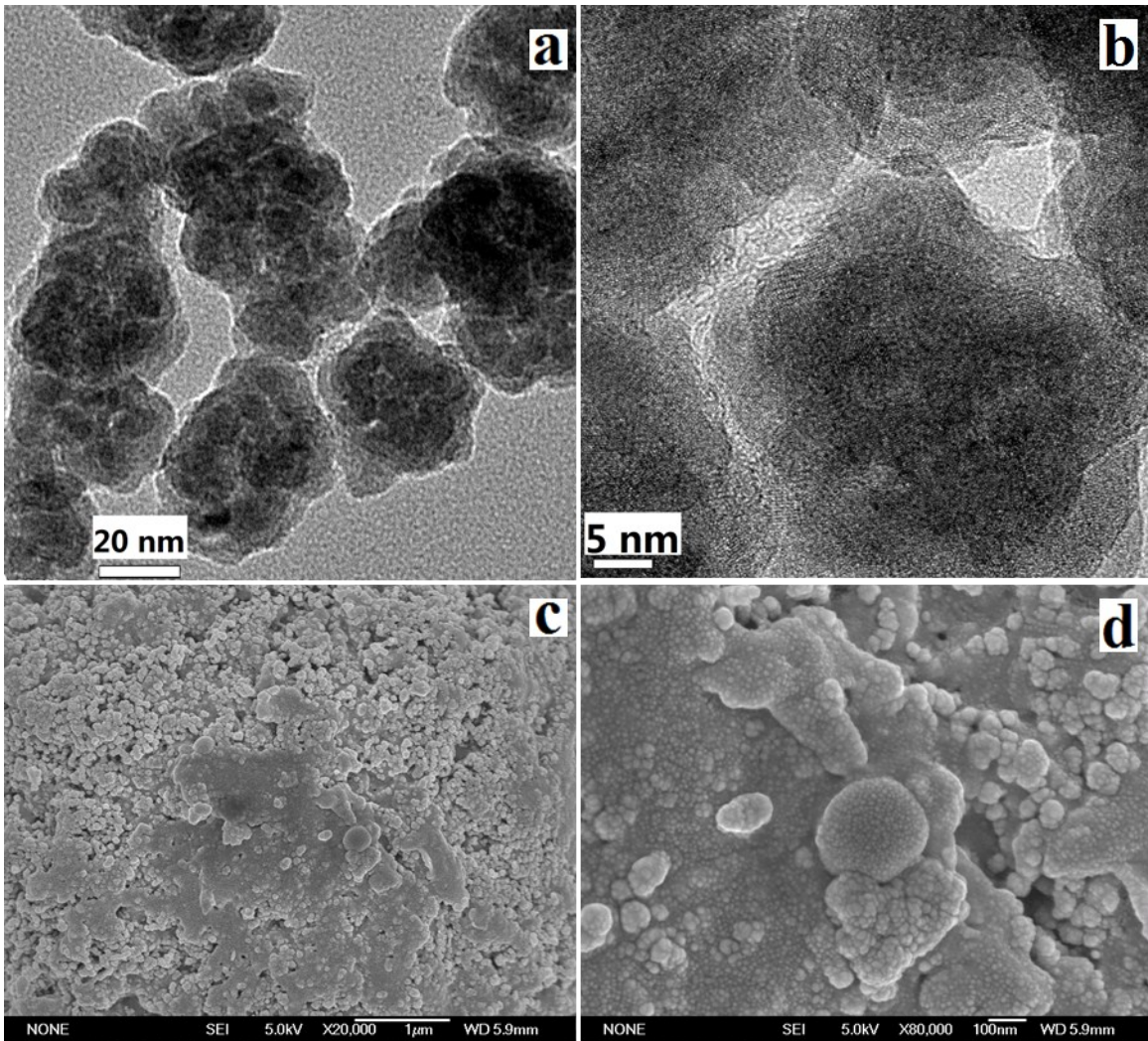


Fig. S9. (a, b) TEM images and (c, d) SEM images of Fe_2O_3 NPs synthesized via thermo-decomposing 3.5 g $\text{Fe}(\text{CO})_5$ in 1.0 g regular PP in 100 mL xylene.

However, the physically adsorbed PP chain on the formed magnetic NPs was only the coordination strength when using regular PP to replace PP-g-MA as evidenced by the random agglomeration shown in TEM and SEM images (Fig. S9). The reason is apparently due to the lack of maleic anhydride groups in PP backbones; which is not strong enough the guide and control the particle growth.

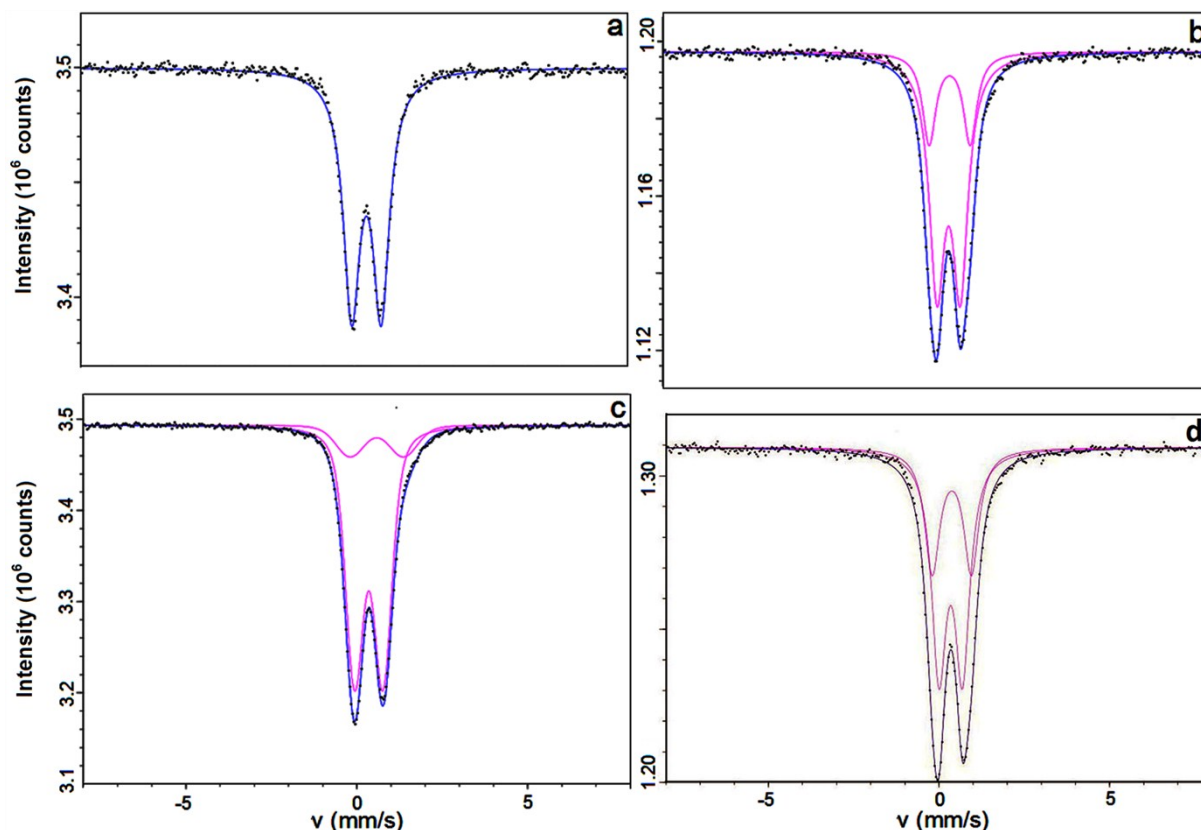


Fig. S10. Room temperature Mössbauer spectra of Fe_2O_3 NPs synthesized via thermodecomposing 3.5 g $\text{Fe}(\text{CO})_5$ in (a). 1.0; (b). 0.5; (c). 0.25; and (d). 0.125 g PP-g-MA in 100 mL xylene.

Room temperature ^{57}Fe Mössbauer spectra were investigated to further confirm the chemical environments of the as-obtained NPs. For the 2-D sheet assembly consisted of mono-dispersed NPs (highest PP-g-MA %, 1.0 g PP-g-MA in 100 mL xylene), only one component was observed as evidenced by an isomer shift (IS) of 0.35 mm/s and quadrupole splitting (QS) of 0.86 mm/s (Fig. S10a), indicating 100% Fe^{3+} in a distorted octahedral oxygen environment.¹¹ The doublet, Fig. S10a, suggests that the Fe_2O_3 NPs are in superparamagnetic states, which agrees well with the negligible coercivity observed in Fig. 3a.¹² For the 3-D porous microspheres (0.5 g PP-g-MA in 100 mL xylene), the Mössbauer spectrum also showed doublet, Fig. S10b. Upon deconvolution, two components were identified: one with IS of 0.35 mm/s, QS of 0.68 mm/s and area of 74 %, suggesting Fe^{3+} in a distorted octahedral oxygen environment; the

other (26% area) with IS of 0.38 mm/s and QS of 1.20 mm/s, indicating Fe^{3+} in more distorted octahedral oxygen environment. The Mössbauer spectrum (Fig. S10c) of the 3-D compressed porous micro-spheres (0.25 g PP-g-MA in 100 mL xylene) showed another two components after deconvolution: one with IS of 0.35 mm/s, QS of 0.83 mm/s and area of 85 %, suggesting Fe^{3+} being in a distorted octahedral oxygen environment; the other (15% area) with IS of 0.58 mm/s and QS of 1.56 mm/s, indicating $\text{Fe}^{2.5+}$ in octahedral site. Doublets corresponding to Fe^{3+} and $\text{Fe}^{2.5+}$ in distorted octahedral oxygen environment most probably represent iron in very small particles, which was confirmed by the SEM and TEM images, Fig. 1&2. Another reason is that iron oxides like hematite and magnetite in bulk are expected to be represented by a sextet in the Mössbauer spectrum. When 1-D Fe_2O_3 nanochains were formed with the lowest PP-g-MA % used (0.125 g PP-g-MA in 100 mL xylene), the Mössbauer spectrum, Fig. S10d, also showed two components after deconvolution: one with IS of 0.35 mm/s, QS of 0.69 mm/s and area of 63 %, suggesting Fe^{3+} being in a distorted octahedral oxygen environment; the other (37% area) with IS of 0.38 mm/s and QS of 1.15 mm/s, indicating Fe^{3+} in more distorted octahedral oxygen environment. Here, the more distorted oxygen environment might contribute to the possible defects that formed upon reducing the PP-g-MA %, which in turn caused the vacancy induced phase transition.¹³ Therefore, the chemical environment of the as-prepared Fe_2O_3 NPs with different assembly patterns controlled by the PP-g-MA % is another possible reason to trigger the change of crystalline structure of Fe_2O_3 NPs.

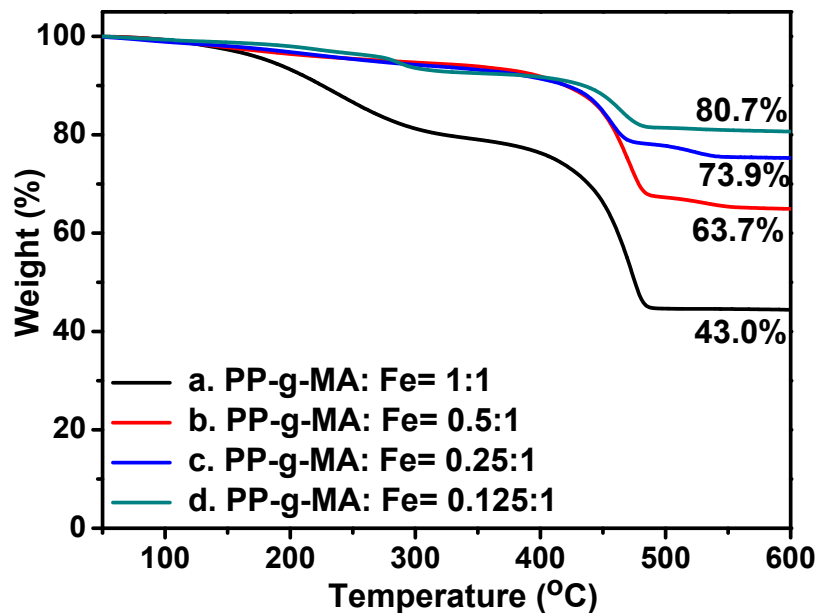


Fig. S11. TGA curves of Fe₂O₃ NPs synthesized via thermo-decomposing 3.5 g Fe(CO)₅ in (a). 1.0; (b). 0.5; (c). 0.25; and (d). 0.125 g PP-g-MA in 100 mL xylene.

The results from Fig. S11 indicated the residue amount was related to the surfactant amount, where the higher PP-g-MA concentration led to the lower residue, and the percentage of the NPs measured in the TGA results agreed well with the measured magnetization property.

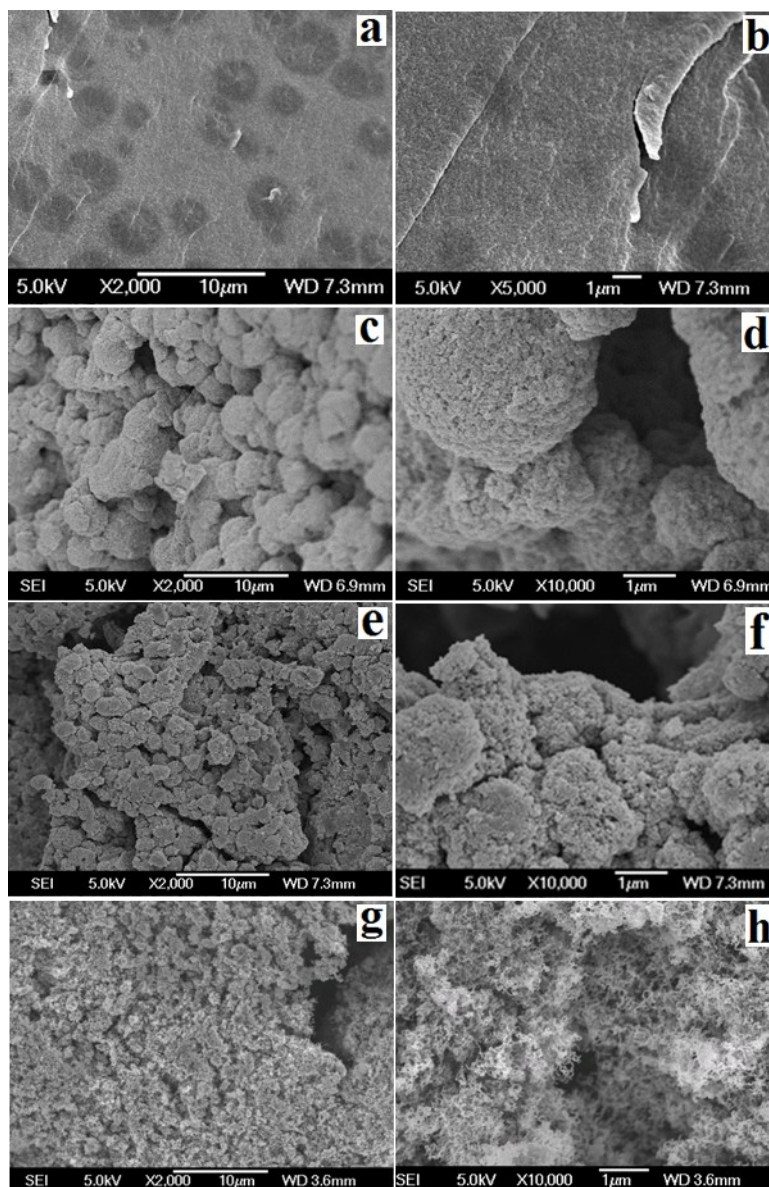


Fig. S12. SEM images of the Fe_2O_3 NPs synthesized via thermo-decomposing 3.5 g $\text{Fe}(\text{CO})_5$ in (a, b). 1.0, (c, d). 0.5, (e, f). 0.25, and (g, h). 0.125 g PP-g-MA in 100 mL xylene.

The assembly patterns of our magnetic system is mainly to be controlled by several key factors: *magnetic di-polar attraction force* from the magnetic moment of Fe_2O_3 , *repulsive force* from the long hydrocarbon chains in the surfactants, *surface tension of the agglomerated particles* within the PP-g-MA matrix during the evaporation of solvent due to different amounts of long hydrocarbon chains when different surfactant concentrations were used. Here,

1. the 2-D sheet micro-structure is mainly attributed to the weak magnetic attraction forces (anti-ferromagnetic α - Fe_2O_3) overcome by the most intensive PP-g-MA repulsive forces due to the highest PP-g-MA concentration;
2. the 3-D porous micro-structure is caused by the stronger magnetic forces which balanced the repulsive force from the surfactant PP-g-MA with intermediate concentrations. And the surface tension of the surfactant lead to the formation of micro-spheres as shown in the SEM images.
3. At last, the 1-D nanochain structure was formed due to the strong magnetic attraction forces (from γ - Fe_2O_3) overcome the weakest repulsive forces (from the lowest surfactant concentration).

Overall, the particle size, assembly pattern (from 1-D nanochain, 2-D sheet to 3-D porous microspheres, Fig. S12), and the crystalline structures (from α - to both α - and γ - phase, and γ - phase Fe_2O_3) can be tuned by simply varying the concentration of PP-g-MA. Strong coordination strength for guiding the particle growth by PP-g-MA is believed to control these as-formed Fe_2O_3 NPs with different crystalline structures and self-assembly patterns. The particle size is increased with decreasing the PP-g-MA % during the thermo-decomposition of the same dose $\text{Fe}(\text{CO})_5$. The main reasons are: when PP-g-MA % was decreased in the colloidal solution, the less strong bonding strength on the particles' surface cannot provide strong enough coordination,¹⁰ which the crystalline structure was altered upon evolved changes in the nuclei density, re-arrangement of stacking sequence, and the defect rearrangement.

Reference

1. E. Frydman, H. Cohen, R. Maoz and J. Sagiv, *Langmuir*, 1997, 13, 5089-5106.
2. N. Wu, L. Fu, M. Su, M. Aslam, K. C. Wong and V. P. Dravid, *Nano letters*, 2004, 4, 383-386.
3. A. L. Willis, N. J. Turro and S. O'Brien, *Chemistry of materials*, 2005, 17, 5970-5975.
4. G. Kataby, M. Cojocaru, R. Prozorov and A. Gedanken, *Langmuir*, 1999, 15, 1703-1708.
5. G. B. Deacon and R. J. Phillips, *Coordination Chemistry Reviews*, 1980, 33, 227-250.
6. M. K. Nazeeruddin, R. Humphry-Baker, P. Liska and M. Grätzel, *The Journal of Physical Chemistry B*, 2003, 107, 8981-8987.
7. J. Rochford, D. Chu, A. Hagfeldt and E. Galoppini, *Journal of the American Chemical Society*, 2007, 129, 4655-4665.
8. L. Li, G. Li, R. Smith Jr and H. Inomata, *Chemistry of materials*, 2000, 12, 3705-3714.
9. I. Battisha, H. Afify and M. Ibrahim, *Journal of magnetism and magnetic materials*, 2006, 306, 211-217.
10. Q. He, T. Yuan, S. Wei, N. Haldolaarachchige, Z. Luo, D. P. Young, A. Khasanov and Z. Guo, *Angewandte Chemie International Edition*, 2012, 51, 8842-8845.
11. S. Hanna, *Science*, 1969, 164, 939.
12. E. Kuzmann, S. Nagy and A. Vertes, *Pure and applied chemistry*, 2003, 75, 801-858.
13. H. Zhu, Y. Ma, H. Yang, C. Ji, D. Hou and L. Guo, *Journal of Physics and Chemistry of Solids*, 2010, 71, 1183-1186.